JOURNAL OF PROPULSION AND POWER
Vol. 27, No. 4, July–August 2011

Fuel-Rich Combustion Characteristics of Biswirl Coaxial Injectors

Kyubok Ahn*
Korea Aerospace Research Institute, Daejeon 305-333, Republic of Korea
Seonghyeon Seo†
Hanbat National University, Daejeon 305-719, Republic of Korea
and
Hwan-Seok Choi‡
Korea Aerospace Research Institute, Daejeon 305-333, Republic of Korea

DOI: 10.2514/1.B34121

An experimental study was performed to investigate the combustion characteristics of liquid–liquid swirl coaxial injectors in fuel-rich conditions. Liquid oxygen and kerosene (Jet A-1) were burned in a range of mixture ratios (0.29–0.41) and chamber pressures (46–65 bar) in a gas generator for a liquid rocket engine. An injector head was connected to a water-cooled chamber and a short nozzle with or without an extension pipe between the chamber and the nozzle. The extension pipe acoustically simulated a turbine inlet manifold. The injector head had 37 identical swirl coaxial injectors. It is found that the characteristic velocity and combustion gas temperature are seldom influenced by the extension pipe, but are only functions of the mixture ratio. The dynamic pressure data show that the combustion instability in the fuel-rich gas generator equipped with biswirl coaxial injectors can be significantly affected by the mixture ratio and also by the extension pipe, which influences the resonant frequency in the chamber.

Nomenclature

C_d	=	discharge coefficient
c	=	speed of sound, m/s
c^*	=	characteristic velocity, m/s
d_n	=	diameter of injector nozzle, mm
$d_{o,o}$	=	diameter of outer oxidizer post, mm
d_s	=	diameter of injector swirl chamber, mm
d_t	=	diameter of injector tangential hole, mm
F_{peak}	=	peak frequency, Hz
l_r	=	injector recess length, mm
m	=	mass flow rate, kg/s
n	=	number of injector tangential hole
OFR	=	oxidizer-to-fuel mixture ratio
p_c	=	chamber pressure, bar
p'_c	=	pressure fluctuation in combustion chamber, bar
p'_{fm}	=	pressure fluctuation in fuel manifold, bar
p'_{om}	=	pressure fluctuation in oxidizer manifold, bar
T_{avg}	=	average temperature of combustion gas, K
Δp_{inj}	=	pressure differential through injector, bar

Subscripts

f	=	fuel
o	=	oxidizer
rms	=	root mean square

I. Introduction

IN A turbopump-fed liquid rocket engine, a gas generator (or preburner) burns propellants and supplies hot gases to drive the turbine blades of a turbopump. The burned gas temperature in the gas generator should be maintained below 900 to 1400 K to prevent uncooled turbine blades from melting or damage according to material limitation [1]. A low gas temperature is usually obtained by either fuel-rich or oxidizer-rich combustion far from the stoichiometric mixture ratio. In spite of some advantages in oxidizer-rich staged combustion cycle engines, a fuel-rich combustion technique has been widely preferred, due to the oxidizing nature of combustion gases in oxidizer-rich operating conditions [2,3].

Combustion-chamber volume and length are determined considering combustion gas residence time. The residence time and characteristic length in a gas generator is generally longer compared with that in a thrust chamber because of low vaporization rates of liquid propellants at lower temperature and requirements for uniform temperature distribution [4]. A gas generator also has no sonic throat, but the turbine nozzles play the role of a choke [5]. Thus, the acoustics of the gas generator, turbine manifold, and nozzle assembly should be simultaneously considered, and the ratio of the entire chamberlike length to chamber diameter in a gas generator becomes higher.

When developing a gas generator, combustion instability has been one of the most serious problems limiting a liquid propellant rocket engine's reliability [6]. Previous researchers reported that they encountered combustion instability during development tests for gas generators [7–12]. Lawver [7] presented abundant data relating to characteristic velocity, gas temperature uniformity, and stability from fuel-rich/oxidizer-rich preburners with like-on-like impinging injectors and platelet injectors using liquid oxygen (LOX) and rocket propellant-1 (RP-1). Combustion instabilities which occurred in the first and second longitudinal modes were effectively damped by adding a turbulence ring and by changing the combustor length. Nesman and Dennis [8] found that the gas generator equipped with fuel-oxidizer-fuel impinging injectors using LOX and RP-1 had significant pressure oscillations at chamber pressures below 18 bar (47% of nominal). At nominal power levels, high-amplitude discrete oscillations occurring in the chamber-alone configuration disappeared in the full gas generator configuration, which included the turbine inlet manifold. They concluded that the oscillations were dependent on the gas generator length and hot gas sound speed, consistent with longitudinal acoustic modes of the gas generator. In another example, as the mixture ratio was lowered, the pressure fluctuations built up in the gas generator with like-on-like injectors using nitrogen tetroxide and Aerozine 50 [9]. Other instability phenomena in gas generators using different propellants and injector designs can be found in [10–12]. From previous research, it is

Received 17 September 2010; revision received 13 February 2011; accepted for publication 15 February 2011.

*Senior Researcher, Combustion Chamber Department, 115 Gwahangno, Yuseong.
†Assistant Professor, Division of Mechanical Engineering, Duckmyoung-dong 16-1, Yuseong.
‡Principal Researcher, Combustion Chamber Department, 115 Gwahang-no, Yuseong.

inferred that combustion instability in a gas generator is more vulnerable to the longitudinal mode, due to its high length-to-diameter ratio, and can be affected by acoustic mode and heat release zone according to chamber length, mixture ratio, injector design, etc.

Longitudinal mode combustion instabilities have been thoroughly studied [5,6,13–16]. As the chamber length increased, the operation repeatedly alternated between unstable and stable in the longitudinal modes [13]. Recently, combustion experiments in a single-element combustor with a gas-centered liquid swirl coaxial injector and their acoustic analysis were performed [14–16]. They suggested that the stability behavior was the result of the combined effects of chamber mode shape and driving combustion mechanism that limited the frequency range over which instability occurred.

In the present study, fuel-rich combustion of LOX and kerosene in a gas generator equipped with biswirl coaxial injectors was experimentally investigated. The gas generator was tested in a chamber-alone configuration and also in combination with an extension pipe acoustically simulating a turbine inlet manifold. The hot combustion gas discharged through a small converging nozzle into ambient atmosphere instead of turbine nozzles. The final assembly configuration of the gas generator, the connecting pipe and the turbine inlet manifold was reported in [12]. The turbine manifold has a broken doughnutlike shape with 11 sonic nozzles.

The injector, which influences atomization, vaporization and mixing of propellants, is known to be most important in combustion performance and stability [2]. For biswirl coaxial injectors using LOX and Jet A-1, injector design parameters such as recess length significantly affected combustion dynamics in thrust-chamber-like unielement and multi-element combustors [17,18]. Though LOX and kerosene biswirl coaxial injectors have been used in gas generators of Russian engines, detailed information on their stability characteristics in fuel-rich combustion conditions is hard to be found in the open literature. Therefore, the objective of the present study is to understand the combustion characteristics in the fuel-rich gas generator equipped with LOX–kerosene biswirl coaxial injectors. The oxidizer-to-fuel mixture ratio, chamber pressure, and chamber axial dimension were the key parameters during the hot-firing tests. The outcome of this experimental work will assist in designing swirl coaxial injectors and gas generators and will also provide the continuing quantitative database for numerical simulation researchers for model validation.

II. Experimental Method

A. Experimental Hardware

Two different types of gas generator configurations were tested in this experiment. The first gas generator model (GG no. 1) has a chamber-alone configuration. The gas generator hardware consists of an injector head, a combustion chamber, and a choked nozzle, as illustrated from left to right in Fig. 1a. The combustion chamber has a cylindrical part, an instrument ring, and a converging part. The internal diameter and the cylindrical length of the combustion chamber are 95 mm and 180 mm, respectively. The exit diameter of the chamber converging part is 51.7 mm and the nozzle throat diameter is 28.4 mm. The length from the injector faceplate to the nozzle throat inlet is 264 mm. The instrument ring is ported for dynamic pressure, static pressure, and temperature sensors. All the components are bolted together and sealed with inserted copper gaskets. During hot-firing tests, water passed through cooling channels enclosed by the cylindrical inner wall and the embossed outer wall.

The second gas generator model (GG no. 2) uses an extension pipe, which is installed between the combustion chamber and the nozzle of the first gas generator model, as shown in Fig. 1b. The extension pipe, acoustically simulating the longitudinal mode of the turbine inlet manifold, expands the chamber length and modifies the acoustics in the chamber. The present pipe length and its diameter are 225 and 51.7 mm, respectively. A connecting adapter is inserted between the pipe and the nozzle. The length from the injector faceplate to the nozzle throat inlet is 499 mm, approximately twice that of the first gas generator model. During gas generator component testing, some extension pipes with different lengths were used instead of the turbine manifold [12,19]. The extension pipe is also bolted together.

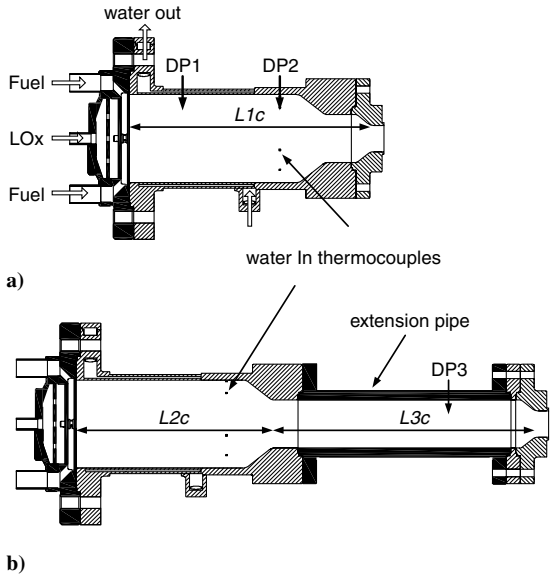

Fig. 1 Schematic of gas generator models: a) GG no. 1 and b) GG no. 2.

The injector head has 37 identical swirl coaxial injectors, which are distributed uniformly along four concentric locations: 1) one at the center, 2) six on the first row, 3) 12 on the second row, and 4) 18 on the third row. Similar to previous research using biliquid swirl coaxial injectors [12,18], LOX flows into the swirling chamber through three tangential holes, forms a swirling motion, and discharges through the inner post of the injector. Kerosene (Jet A-1) is supplied via four tangential holes and passes through the outer post into the combustion chamber. The injector's geometric dimensions are summarized in Table 1.

B. Experimental Condition

Static pressure and temperature measurements in propellant manifolds and combustion chamber were made using pressure transducers and type-K thermocouples, respectively. To obtain a temperature distribution of combustion gases, five thermocouples were installed in the instrument ring: one was at the center, one was in the vicinity of the inner wall, and others were on the circle corresponding to the half-area of the cross section. They were recorded at a rate of 100 Hz using a data-acquisition system.

To evaluate the combustion dynamics, piezoelectric-type dynamic pressure sensors were used as the main detectors in the propellant manifolds and the combustion chamber. Two or three water-cooled helium-bleed piezoelectric dynamic pressure sensors were mounted on the combustion chamber and extension pipe as depicted in Fig. 1. Pressure fluctuations in the oxidizer manifold and the fuel manifold were measured by piezoelectric-type sensors. Pressure fluctuation

Table 1 Specifications of biswirl coaxial injectors used in the present study

Parameter	Value
$d_{t,f}$	1.2 mm
$d_{t,o}$	1.1 mm
$d_{s,f}$	4.5 mm
$d_{s,o}$	3.5 mm
$d_{o,o}$	2.5 mm
$d_{n,f}$	4.5 mm
$d_{n,o}$	1.5 mm
n_f	4
n_o	3
l_r	1.4 mm

Table 2 Hot-firing test conditions

Test no.	Extension pipe	m_o, kg/s	m_f, kg/s	OFR	p_c, bar	$\Delta p_{\text{inj},o}$, bar	$\Delta p_{\text{inj},f}$, bar	c, m/s
GG no. 1-1	No	1.09	3.19	0.34	50.3	16.6	10.6	652
GG no. 1-2	No	1.10	3.31	0.33	52.8	13.6	9.7	642
GG no. 1-3	No	1.03	3.45	0.30	54.4	12.9	10.2	615
GG no. 1-4	No	0.87	2.95	0.30	46.4	9.1	7.2	615
GG no. 1-5	No	0.93	2.27	0.41	50.7	7.3	3.1	705
GG no. 1-6	No	1.02	3.05	0.34	54.3	12.4	7.8	646
GG no. 2-1	Yes	1.09	3.07	0.35	57.0	9.0	6.9	660
GG no. 2-2	Yes	1.18	3.29	0.36	58.4	10.4	7.8	662
GG no. 2-3	Yes	1.13	3.48	0.32	56.1	9.7	8.6	635
GG no. 2-4	Yes	1.16	3.19	0.36	57.5	9.5	6.8	666
GG no. 2-5	Yes	1.13	3.31	0.34	56.3	9.4	7.6	650
GG no. 2-6	Yes	1.10	3.77	0.29	55.1	10.0	10.1	610
GG no. 2-7	Yes	1.18	2.99	0.40	58.1	9.8	6.2	693
GG no. 2-8	Yes	0.97	2.81	0.35	48.2	7.3	6.0	657
GG no. 2-9	Yes	1.30	3.79	0.34	64.3	12.6	10.4	649

was sampled at 50 kHz using a high-frequency data-acquisition system.

The 15 tests were conducted with chamber pressures ranging from 46 to 65 bar and oxidizer-to-fuel mixture ratios ranging from 0.29 to 0.41. The test conditions such as chamber pressure (p_c), oxidizer-side pressure drop in the injector ($\Delta p_{\text{inj},o}$), fuel-side pressure drop ($\Delta p_{\text{inj},f}$), oxidizer-to-fuel mixture ratio (OFR), and propellant mass flow rate (m_o and m_f) are summarized in Table 2. Static pressure and mass flow rate data in 1 s, 100 samples, were averaged during the steady-state condition [18]. The oxidizer-to-fuel mixture ratio, chamber pressure, and chamber axial dimension were the key parameters affecting the combustion characteristics during hot-firing tests. Ignition was achieved with a gaseous oxygen/gaseous methane torch igniter. Combustion usually lasted for 4 s, which was enough to acquire data of static and dynamic combustion characteristics. Pressure and mass flow rate measurement uncertainties were confirmed to be less than 0.25% in the area of interest.

III. Result and Discussion

A. Injector Spray Characteristics

Atomization and spray characteristics of propellants are significantly related to combustion performance and combustion stability. The swirl injector is well known for uniform spray distribution and homogeneous drop size. Before conducting hot-firing tests, hydraulic tests on the present swirl coaxial injector were performed in advance for obtaining spray cone angles and understanding mixing characteristics of the propellants. The photographs in Fig. 2 are the instantaneous spray patterns taken using a charge-coupled-device camera and a strobe light. Each pattern shows the sprays through the oxidizer injector only, the fuel injector only, and mixed oxidizer/fuel injectors. As simulant of the propellants, tap water was used to obtain the images. At this time, pressure differentials and mass flow rates through the fuel injector/oxidizer injector were 10.9/9.4 bar and 100/29 g/s, respectively.

From each image in Fig. 2, the spray cone angles are 61.0, 86.8, and 83.6 deg from left to right. Considering the measured spray angles, it can be confirmed that two spray sheets meet outside the injector and the present injector has external mixing characteristics. As opposed to the clear distinction of individual oxidizer and fuel sprays in the external mixing swirl coaxial injector for a liquid rocket thrust chamber [17], it is difficult to distinguish individual sprays in the mixed condition. The oxidizer-to-fuel mixture ratio in the injector of the thrust chamber is around nine times higher than that of the gas generator [18]. Thus, the dense outer spray from the fuel injector is thought to block the visualization of the inner spray from the oxidizer injector. Kim [20] reported that the merged coaxial spray angle was greatly influenced by the relative momentum change of the inner and outer liquid sheets. In this case, since the fuel mass flow rate is about three times larger than the oxidizer flow rate, the spray through the inner oxidizer injector is moved outwards and combined with the fuel spray. Thus, the spray angle of the mixed spray almost approaches the spray angle of the outer fuel spray. By the definitions of Soltani et al. [21], the swirl numbers for the inner oxidizer injector and for the

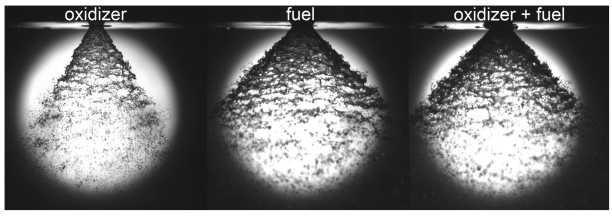

Fig. 2 Instantaneous backlit images of spray from the present swirl coaxial injector.

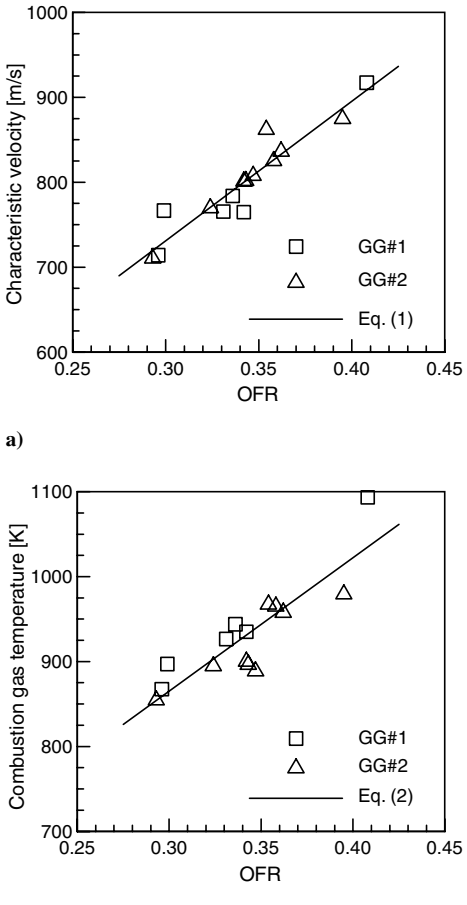

Fig. 3 Plots of a) characteristic velocities and b) average combustion gas temperature.

outer fuel one in the present study are calculated as 1.84 and 1.99, respectively.

B. Static Combustion Characteristics

Characteristic velocities acquired from hot-firing tests are presented in Fig. 3a as a function of mixture ratio. As expected from the previous research [7,9,12], the characteristic velocity has a linear relationship with the mixture ratio, but is not a strong function of chamber pressure and chamber length within the present experimental conditions from OFR = 0.29 to OFR = 0.41. The empirical equation for the characteristic velocity c^* in the present study is

$$c^* = 1644.6 \times \mathrm{OFR} + 237.6 \tag{1}$$

This equation is similar to the ones derived in the previous studies using LOX and hydrocarbon fuels [7,12] and has slightly different constants, due to differences in measurement location, operating conditions, kerosene constituents, etc.

The average temperature of the combustion gases in the combustion chamber was calculated by the area weighted average from the five thermocouples installed in the instrument ring. All average gas temperature data are depicted in Fig. 3b. The average temperature is also seen to be nearly proportional to the mixture ratio. In the range of high mixture ratios over 0.4, the gas temperature shows some discrepancies from the fitting line. The damage of one or two thermocouple probes due to high temperatures could have induced measurement errors in averaging. The empirical equation of average gas temperature in the present study is

$$T_{\mathrm{avg}} = 1570.4 \times \mathrm{OFR} + 394.1 \tag{2}$$

The obtained average temperature data showed good agreement with the previous experimental result [7] and numerically predicted result [22], which presented a linear relationship between mixture ratio and gas temperature in fuel-rich combustion from OFR = 0.3 to 0.4.

During the hot-firing tests, the discharge coefficients of the fuel and the oxidizer sides through the injector were measured and presented in Fig. 4. Though the GG no. 1 and the GG no. 2 used the same injector head, the discharge coefficient of the oxidizer side changed a great deal and that of the fuel side varied a little, which meant that there were very different combustion phenomena between them. As found in the previous research [3,8], the low values of discharge coefficients through the oxidizer-side injector in the GG no. 1 are believed to be related with longitudinal mode combustion instability, which will be discussed in the next section.

C. Dynamic Combustion Characteristics

Raw dynamic pressure data sampled at 50 kHz were digitally filtered by a bandpass of 50 and 10,000 Hz to eliminate direct current components and noise. The time history of the filtered dynamic pressures for the GG no. 1-1 test is plotted in Fig. 5, which shows a limit-cycle oscillation. The first and second dynamic pressure sensors, DP1 and DP2, were located at 60 and 162 mm, respectively, downstream from the injector faceplate. DP1 was flush-mounted on the inner surface of the combustion chamber, but DP2 was mounted with a 40 mm recess, due to the space limitation of the instrument ring. Assuming that the characteristic length of the combustion chamber is the length ($L1_C = 264$ mm) from the injector face plate to the nozzle throat inlet, as shown in Fig. 1a, DP2 is downstream at half the characteristic length. Even though the first longitudinal mode combustion instability took place, both signals at DP1 and DP2 moved in phase. This means that temperature was not axially uniform

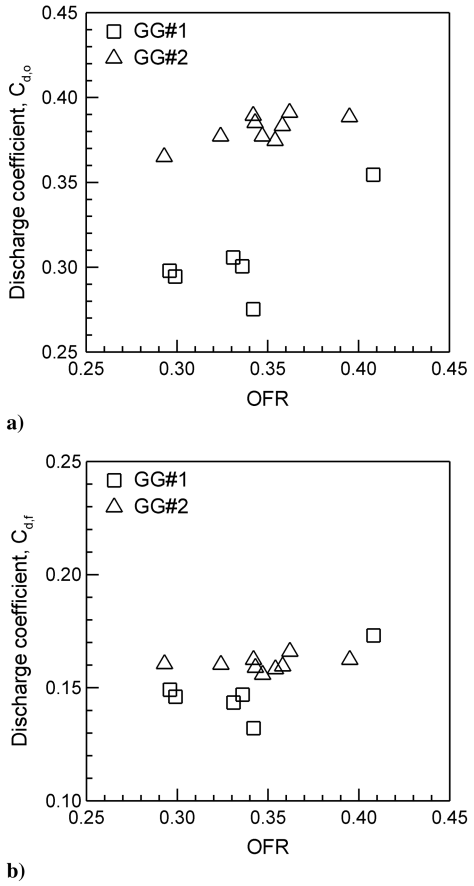

Fig. 4 Discharge coefficients through the injectors under hot-firing tests: a) oxidizer side and b) fuel side.

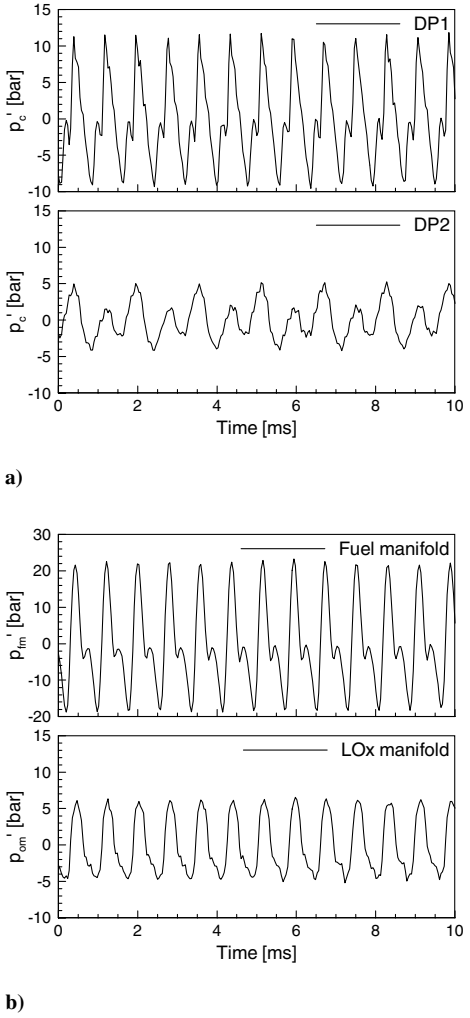

Fig. 5 Time histories of the filtered dynamic pressures for the GG no. 1-1 test.

in the combustion chamber and thus temperature distribution affected the acoustic mode shape [15]. The filtered pressure fluctuation data in both manifolds also have large amplitude and are somewhat phase-delayed with those in the combustion chamber. Based on the DP1 signal near the pressure antinode, the peak-to-peak amplitude of the pressure oscillation is found to be 20 bar, which is about 40% of the corresponding chamber pressure. The dynamic pressure at DP1 looks like a sinusoidal wave with steep slopes, due to nonlinear effects. The signal at DP2 represents a more complex pattern, which has a high-amplitude wave in one period and a low-amplitude wave in the next period. The acoustic resonance in the long recess passage seems to influence pressure measurements at DP2 [23]. The amplitude of the pressure fluctuations in the fuel manifold was approximately four times higher than that in the oxidizer manifold, since the fuel mass flow rate was three times larger than the oxidizer one.

For the analysis of the data in the frequency domain, the power spectral density was calculated using fast Fourier transform analysis. Sampling frequency, number of points in the Fourier transforms, and number of blocks used in the ensemble average were 50 kHz, 25,000, and 8, respectively [18]. The power spectral densities in the combustion chamber for the GG no. 1 are presented in Fig. 6. The results obviously showed that there were strong resonant pressure oscillations in the chamber through all the tests. Except for the GG no. 1-5 test, the first longitudinal mode resonant frequencies in the vicinity of 1200 Hz and their harmonic frequencies are seen clearly. As compared with the power spectral densities at DP1, the power spectral densities at DP2 show subharmonic frequencies with relatively small values in the vicinity of 600 Hz as well as the first longitudinal mode frequencies around 1200 Hz. This can be expected from the filtered dynamic pressure data in Fig. 5a. Except for the GG no. 1-5 test, all the patterns of the power spectral densities look very

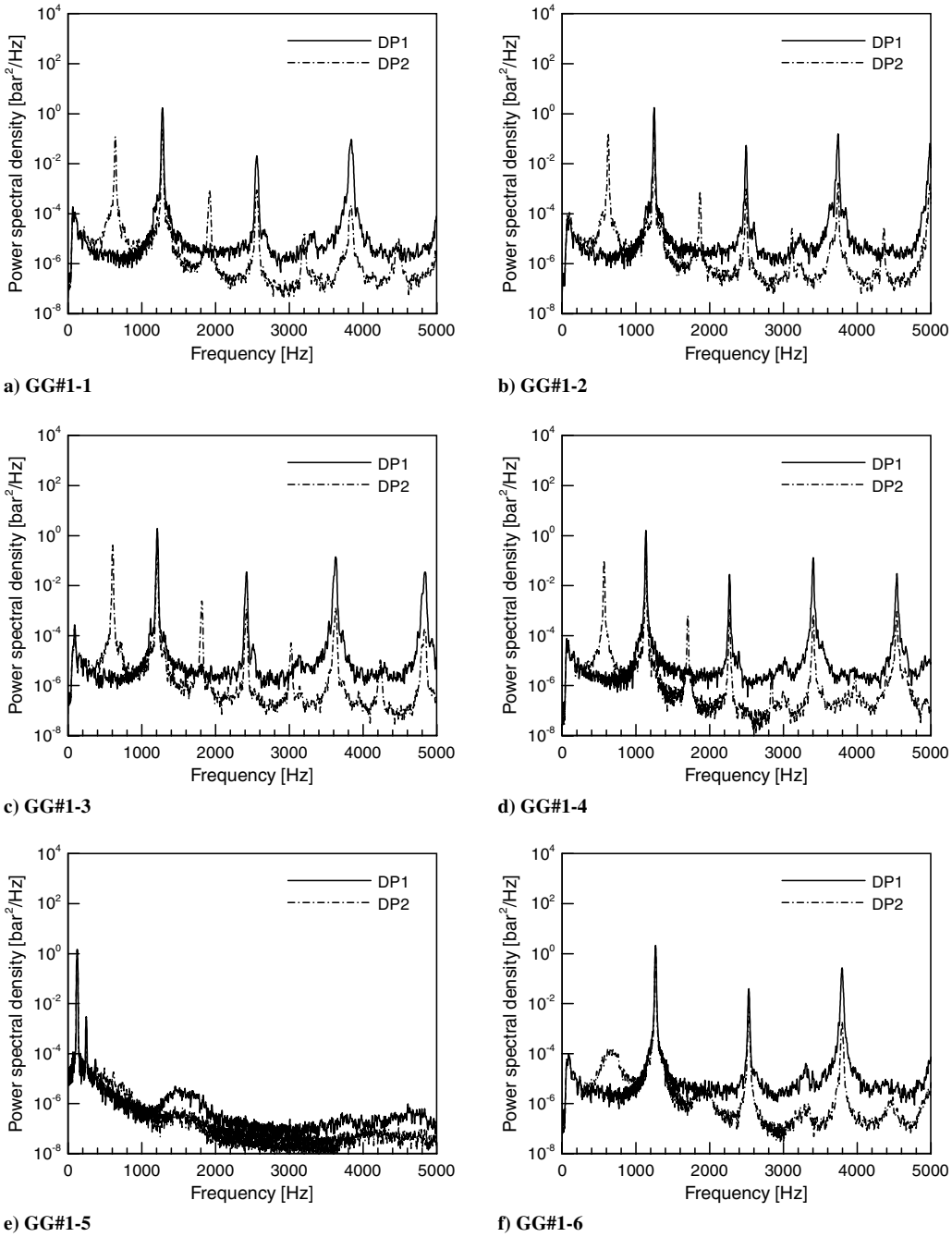

Fig. 6 Power spectral densities of pressure fluctuations in the GG no. 1 combustion chamber.

similar, although variations of combustion gas temperature affected the resonant frequencies.

In the case of the GG no. 1-5 test, the low-frequency combustion instability with the highest peak in the vicinity of 120 Hz is introduced, as shown in Fig. 6e. The peak frequency is well below the lowest resonant frequency in the combustion chamber. From Table 2, at this time, OFR is 0.41 and $\Delta p_{\text{inj},f}$ is 3.1 bar, which is only 6% of the corresponding chamber pressure. When the pressure differential through the injector is very low, the propellant supply system and combustion chamber may correspond acoustically [5]. The filtered pressure fluctuation in the chamber and manifolds for the GG no. 1-5 test are presented in Fig. 7. The dynamic pressure data show an apparent sinusoidal wave shape and also the amplitudes of the filtered fluctuations are almost the same through the manifolds and the chamber. The pressure wave at DP1 has no phase delay with those at DP2 and at the fuel manifold, but has a phase delay of around 30 deg with that at the oxidizer manifold. Seo et al. [12] reported that the low-frequency instability in a fuel-rich gas generator equipped with swirl coaxial injectors using LOX and kerosene could occur at chamber pressures below the critical pressure of oxygen. However, at this time, the chamber pressure is 50.7 bar, which is the supercritical pressure of oxygen. From these results, it is apparent that bulk-mode combustion instability was encountered during the GG no. 1-5 test.

To understand the relationship between the peak frequency with the maximum power spectral density and the mixture ratio, the highest peak frequencies obtained in the combustion chamber are plotted in Fig. 8a. Except for the case of the GG no. 1-5 test, the empirical equation of the peak frequencies obtained from both DP1 and DP2 can be acquired as follows:

$$F_{\text{peak}} = 2701.3 \times \text{OFR} + 355.9 \tag{3}$$

where the highest peak frequencies outside the range of the first longitudinal mode were not considered. It is certain that the peak frequency in the vicinity of the first longitudinal mode is a function of mixture ratio, since the mixture ratio determines the combusted gas temperature in the combustion chamber. The speed of sound for each test is obtained using the adiabatic index and molar mass calculated from the Chemical Equilibrium Analysis (CEA) code [24] and average temperature of the combustion gas from Eq. (2). The calculated speed of sound is listed in Table 2. Then, from the sonic velocity and the characteristic length ($L1_C = 264$ mm), the first longitudinal mode resonant frequency can be calculated. Again, by correlating the calculated frequency and the measured OFR in Table 2, the following linear equation can be derived and plotted in Fig. 8a:

$$F_{\text{peak}} = 1545.5 \times \text{OFR} + 705.1 \tag{4}$$

Though Eqs. (3) and (4) have very different constants, the two equations are found to be well matched over the range of OFRs from 0.275 to 0.425, as shown in Fig. 8a. This confirms that the combustion instabilities in the GG no. 1 occurred in the first longitudinal mode with the pressure antinodes at the injector faceplate and the nozzle throat inlet. Percentage of the rms value of the filtered dynamic pressure normalized by the chamber pressure and maximum power spectral densities at the DP1 during hot-firing tests in the GG no. 1 are depicted in Fig. 8b. The rms values have approximately 10% of the corresponding chamber pressures, and the maximum power spectral densities are around 2 bar^2/Hz through all

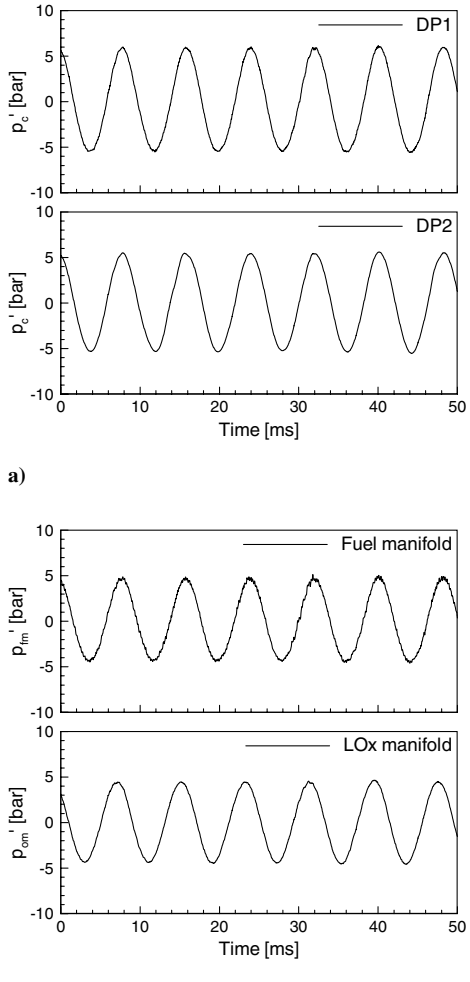

Fig. 7 Time histories of the filtered dynamic pressures for the GG no. 1-5 test.

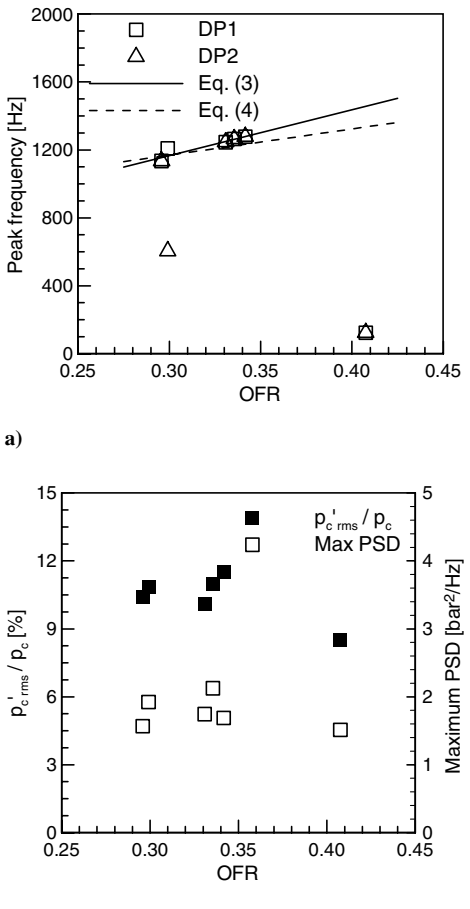

Fig. 8 Plots of a) peak frequencies and b) rms values of pressure fluctuations normalized by chamber pressure in the GG no. 1 combustion chamber.

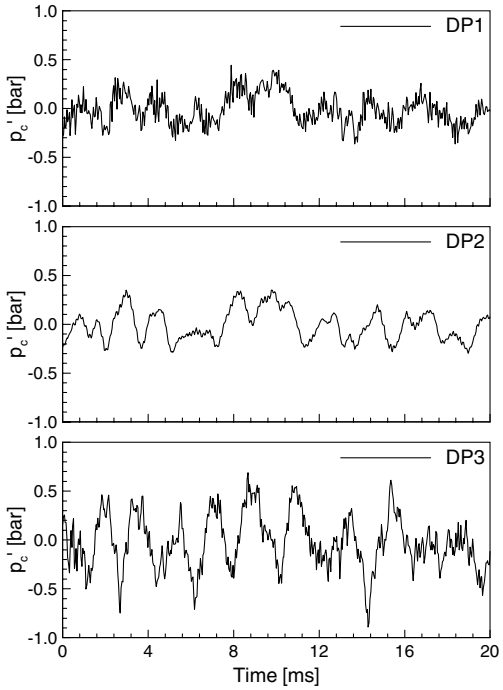

Fig. 9 Time histories of the filtered dynamic pressures for the GG no. 2-1 test.

the tests. Combustion stability in a liquid rocket engine has been extensively reviewed in the literature [5,25]. Klem and Fry [25] have reported that from the standpoint of combustion instability an engine should operate without sustained peak-to-peak pressure oscillations over 10% of the mean chamber pressure. According to their criterion, all the operating conditions in the GG no. 1 can be said to have been unstable.

As a next step, a series of combustion tests with the GG no. 2 were performed in order to investigate the effect of the extension pipe on the combustion dynamics. The additional dynamic pressure transducer (DP3) was flush-mounted in the extension pipe, 394 mm downstream of the injector face plate, as shown in Fig. 1b. The time history of the filtered dynamic pressures for the GG no. 2-1 test is plotted in Fig. 9, which shows very-low-amplitude oscillations compared with the GG no. 1-1 test. From all the signals in the combustion chamber, the peak-to-peak amplitude of the pressure oscillation is found to be 1 bar, which is less than 2% of the corresponding chamber pressure. It is noteworthy that the dynamic pressure at DP3 has a different wave shape from those at DP1 and DP2. It indicated that the dominant resonant frequency in the extension pipe was not the same as that in the combustion chamber, i.e., between the injector face plate and the exit of the chamber converging part.

For in-depth analysis of the data, the power spectral densities of the filtered dynamic pressure data were calculated as presented in Fig. 10. Since the results at DP2 are similar to those at DP1, only the power spectral densities at DP1 and DP3 are plotted. Except for the GG no. 2-6 test, Fig. 10 obviously showed that there were not strong resonant pressure oscillations in the chamber, although some resonant frequencies could still be seen. As expected from Fig. 9, the highest peaks at DP3 have different frequencies from those at DP1. Except for the GG no. 2-6 test, all the patterns of the power spectral densities seem very similar for one another and have more complex peaks compared with those in the GG no. 1, due to several characteristic lengths. The combustion instability was encountered only at the GG no. 2-6 test during the hot-firing tests of the GG no. 2. In the case of the GG no. 2-6 test, the first longitudinal mode resonant

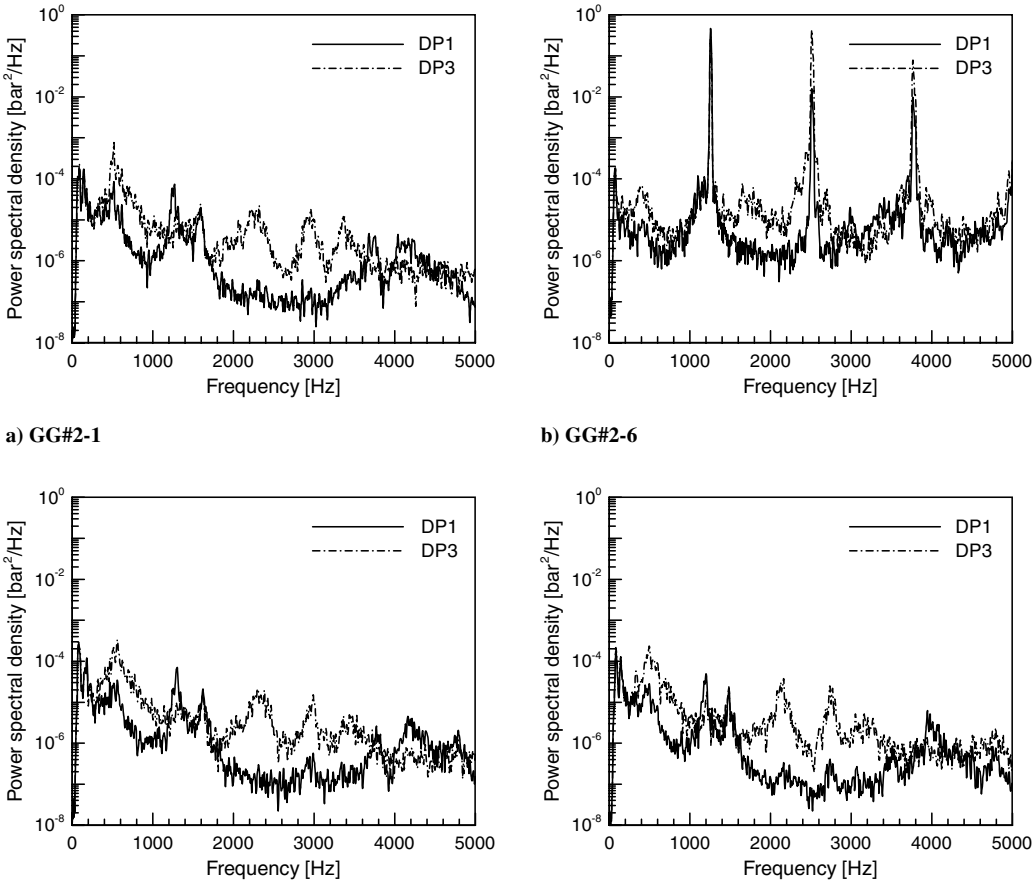

a) GG#2-1 **b) GG#2-6**

c) GG#2-7 **d) GG#2-8**

Fig. 10 Power spectral densities of pressure fluctuations in the GG no. 2 combustion chamber.

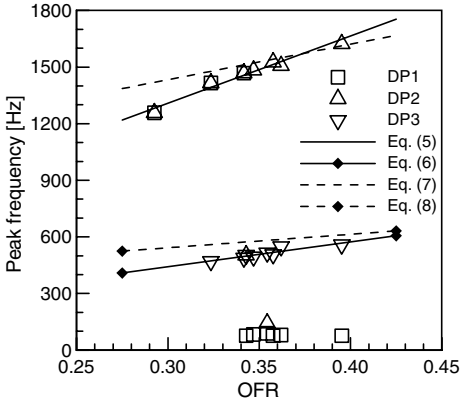

a)

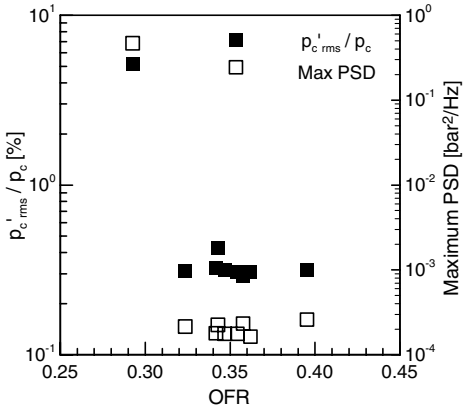

b)

Fig. 11 Plots of a) peak frequencies and b) rms values of pressure fluctuations normalized by chamber pressure in the GG no. 2 combustion chamber.

frequency near 1200 Hz and their harmonic frequencies are found clearly at DP3 as well as at DP1.

Similar to the analysis of the GG no. 1 tests, the highest peak frequencies obtained in the combustion chamber for the GG no. 2 were calculated as shown in Fig. 11a. Some cases have very low peak frequencies extrinsic to the acoustic frequencies, since the amplitudes at the resonant mode frequencies are below the noise level at low frequency. Considering the highest peak frequencies inside the range of the resonant mode, the empirical equation of the peak frequencies obtained from DP1 and DP2 can be acquired as follows:

$$F_{\text{peak}} = 3568.6 \times \text{OFR} + 237.1 \tag{5}$$

The empirical equation of the peak frequencies obtained from DP3 can be acquired as follows:

$$F_{\text{peak}} = 1315.7 \times \text{OFR} + 46.4 \tag{6}$$

We assume that the characteristic length ($L2_C = 215$ mm) at DP1 and DP2 is the length from the injector face plate to the exit of the chamber converging part as the closed-end/closed-end system and the characteristic length ($L3_C = 284$ mm) at DP3 is the length from the exit of the chamber converging part to the nozzle throat inlet as the open-end/closed-end system. Using the same method used to calculate Eq. (4), the first longitudinal mode resonant frequency of the characteristic length ($L2_C$) can be calculated. Comparing the calculated frequency and the measured OFR in Table 2, the following linear equation at DP1 and DP2 is acquired and plotted in Fig. 11a:

$$F_{\text{peak}} = 1886.5 \times \text{OFR} + 866.8 \tag{7}$$

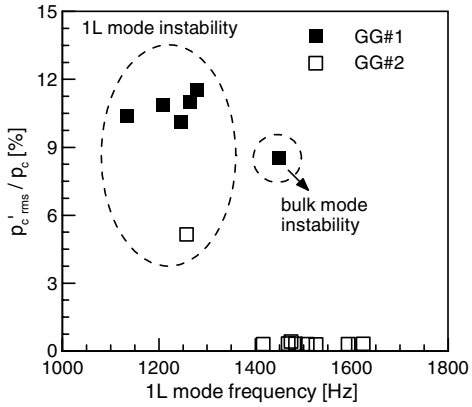

Fig. 12 Root-mean-square values of pressure fluctuations normalized by chamber pressure as a function of the first longitudinal mode frequency.

The linear equation of the resonant frequency of the characteristic length ($L3_C$) at DP3 can be acquired as follows:

$$F_{\text{peak}} = 714.1 \times \text{OFR} + 328.1 \tag{8}$$

Though the constants in Eqs. (7) and (8) have very different values from those in Eqs. (5) and (6), Eqs. (7) and (8) correlates the measured frequencies as shown in Fig. 11. This means that the assumed characteristic lengths ($L2_C$ and $L3_C$) are reasonable. The percentage of the rms value of the filtered dynamic pressure normalized by the chamber pressure and maximum power spectral densities at DP1 during hot-firing tests in the GG no. 2 are depicted in Fig. 11b. Except for the GG no. 2-6 test, the rms values of pressure fluctuations are below 0.5% of the corresponding chamber pressures and the maximum power spectral densities have the order of 10^{-4} bar^2/Hz. The rms value during the GG no. 2-6 test is 5% of the chamber pressure.

To fully understand the combustion instabilities encountered during the hot-firing tests of the GG no. 1 and GG no. 2, the frequencies measured at DP1, corresponding to the first longitudinal mode in the combustion chamber, were analyzed. Then the rms values of the pressure fluctuations in the combustion chamber were normalized by the chamber pressures and expressed as a function of the first longitudinal mode frequency as shown in Fig. 12. The points at which combustion instability occurred are marked in the dashed circles. This shows that the first longitudinal mode combustion instability in the present study is strongly related to the specific frequency range between 1100 and 1300 Hz. According to the time-lag theory [5,26,27], the characteristic time (the combustion time) in the present gas generator equipped with the biswirl coaxial injectors appears to be commensurate with the period of oscillation between 1/1300 s and 1/1100 s. For completeness of the current work, heat release rate measurements performed in [27] are highly recommended as possible future work.

IV. Conclusions

The effects of the extension pipe simulating the turbine inlet manifold on the combustion characteristics in the fuel-rich gas generator with LOX/kerosene biswirl coaxial injectors have been investigated. The current experiment studied over the chamber pressure range from 46 to 65 bar and the oxidizer-to-fuel mixture ratio from 0.29 to 0.41.

Under the present experimental conditions, both the characteristic velocity and the average gas temperature in the combustion chamber showed a nearly linear relationship with the mixture ratio; however, they were insensitive to the chamber pressure and chamber length. When the first longitudinal mode combustion instability took place, the discharge coefficients through the swirl coaxial injectors changed significantly.

The pressure fluctuation data showed that the combustion instabilities occurred during all the tests of the GG no. 1 without the

extension pipe. The first longitudinal mode combustion instabilities took place throughout the tests, except for the GG no. 1-5 test, where the bulk-mode-type instability was encountered. In the GG no. 1 combustion chamber, the rms values of the filtered dynamic pressures were approximately 10% of the corresponding chamber pressures. During the hot-firing tests of the GG no. 2 with the extension pipe, strong pressure oscillations did not occur and the rms values of the filtered dynamic pressures were below 0.5% of the corresponding chamber pressures in the combustion chamber, except for the GG no. 2-6 test, where the first longitudinal mode combustion instability was encountered.

It was found that when the first longitudinal mode frequency existed in the specific range between 1100 and 1300 Hz, the longitudinal mode combustion instability occurred. The characteristic combustion time in the present gas generator with the LOX/kerosene biswirl coaxial injectors appears to have been commensurate with the period of oscillation between $1/1300$ s and $1/1100$ s. Thus, it is important that the oxidizer-to-fuel mixture ratio, combustion-chamber geometry and length of the turbine inlet manifold, which influence the resonant frequency, all need to be carefully selected in rocket chamber design for achieving better combustion stability.

Acknowledgments

The present study is a part of the "Research and Development of Korea Space Launch Vehicle-I" project financially supported by the Ministry of Education, Science and Technology (MEST), and the authors would like to thank the MEST for its support.

References

[1] Sutton, G. P., *Rocket Propulsion Elements: An Introduction to the Engineering of Rockets*, 6th ed., Wiley, New York, 1992, pp. 212–213.

[2] Huzel, D. K., and Huang, D. H., *Modern Engineering for Design of Liquid-Propellant Rocket Engines*, Progress in Aeronautics and Astronautics, Vol. 147, AIAA, Washington, D.C., 1992.

[3] Soller, S., Wagner, R., Kau, H. P., Martin, P., and Mäding, C., "Combustion Stability Characteristics of Coax-Swirl-Injectors for Oxygen/Kerosene," AIAA Paper 2007-5563, 2007.

[4] Zehetner, H. C., "Liquid Propellant Gas Generator," NASA SP-8081, March 1972.

[5] Harrje, D. T., and Reardon, F. H., "Liquid Propellant Rocket Combustion Instability," NASA SP-194, 1972.

[6] Dranovsky, M. L., *Combustion Instabilities in Liquid Rocket Engines: Testing and Development Practices in Russia*, Progress in Astronautics and Aeronautics, Vol. 221, AIAA, Reston, VA, 2007.

[7] Lawver, B. R., "Test Verification of LOX/RP-1 High-Pressure Fuel/Oxidizer-Rich Preburner Designs," *Journal of Spacecraft and Rockets*, Vol. 20, No. 6, 1983, pp. 567–573. doi:10.2514/3.8588

[8] Nesman, T., and Dennis, J., "Fastrac Gas Generator Testing," Tenth Thermal and Fluids Analysis Workshop, NASA Marshall Space Flight Center Rept. 19990105709, Sept. 1999.

[9] Mah, C. S., "Evaluating the Operational Limits of a Gas Generator," AIAA Paper 2001-3990, 2001.

[10] Ito, J. I., "Development of LO_2/LH_2 Gas Generators for the M-1 Engine," NASA CR-54812, 1966.

[11] Huebner, A. W., "High-Pressure LOX/Hydrogen Preburners and Gas Generators," NASA CR-161814, 1981.

[12] Seo, S., Kim, S. K., and Choi, H. S., "Combustion Dynamics and Stability of a Fuel-Rich Gas Generator," *Journal of Propulsion and Power*, Vol. 26, No. 2, 2010, pp. 259–266. doi:10.2514/1.46568

[13] Morgan, C. J., and Sokolowski, D. E., "Longitudinal Instability Limits with a Variable Length Hydrogen-Oxygen Combustor," NASA TN-D-6328, 1971.

[14] Miller, K., Sisco, J., Nugent, N., and Anderson, W., "Combustion Instability with a Single-Element Swirl Injector," *Journal of Propulsion and Power*, Vol. 23, No. 5, 2007, pp. 1102–1112. doi:10.2514/1.26826

[15] Smith, R., Nugent, N., Sisco, J., Xia, G., Anderson, W., Sankarank, V., and Merkle, C. L., "Experimental and Computational Investigation of Combustor Acoustics and Instabilities, Part I: Longitudinal Modes," AIAA Paper 2006-537, 2006.

[16] Sisco, J. C., Smith, R. J., Sankaran, V., and Anderson, W. E., "Examination of Mode Shapes in an Unstable Model Rocket Combustor," AIAA Paper 2006-4525, 2006.

[17] Kim, S. H., Han, Y. M., Seo, S., Moon, I. Y., Kim, J. K., and Seol, W. S., "Effects of LOX Post Recess on the Combustion Characteristics for Bi-Swirl Coaxial Injector," AIAA Paper 2005-4445, 2005.

[18] Ahn, K., Han, Y. M., Seo, S., and Choi, H. S., "Effects of Injector Recess and Chamber Pressure on Combustion Characteristics of Liquid-Liquid Swirl Coaxial Injectors," *Combustion Science and Technology*, Vol. 183, 2011, pp. 252–270. doi:10.1080/00102202.2010.516289

[19] Ahn, K., Lee, K. J., Seo, S., Han, Y. M., and Choi, H. S., "Effect of Combustion Chamber Design on Combustion Stability Characteristics of a Full-Scale Gas Generator," *Journal of the Korean Society of Propulsion Engineers*, Vol. 11, No. 1, 2007, pp. 11–17.

[20] Kim, D., "Spray Characteristics of Swirl Coaxial Type Injectors for Liquid Rocket Engines," Ph.D. Dissertation, Seoul National University, Seoul, ROK, 2007.

[21] Soltani, M. R., Ghorbanian, K., Ashjaee, M., and Morad, M. R., "Spray Characteristics of a Liquid-Liquid Coaxial Swirl Atomizer at Different Mass Flow Rates," *Aerospace Science and Technology*, Vol. 9, 2005, pp. 592–604. doi:10.1016/j.ast.2005.04.004

[22] Lee, C., Yu, J., and Koo, J. Y., "Prediction of Non-Equilibrium Kinetics of Fuel-Rich Kerosene/LOX Combustion in Gas Generator," AIAA Paper 2007-574.

[23] Gosweiller, C., Wilson, B., and Walter, T., "Application of an Improved Model for the Determination of Acoustic Resonances in Indicator Passages for Combustion Pressure Measurements," *ASME 2006 Internal Combustion Engine Division Spring Technical Conference*, ASME International, New York, 2006, pp. 769–779; also Paper ICES2006-1373. doi:10.1115/ICES2006-1373

[24] Gordon, S., and McBride, B. J., "Computer Program for Calculation of Complex Chemical Equilibrium Compositions and Applications," NASA Ref. Publ. 1311, 1996.

[25] Klem, M. D., and Fry, R. S., "Guidelines for Combustion Stability Specifications and Verification Procedures for Liquid Propellant Rocket Engines," Chemical Propulsion Information Agency, Publ. 655, Columbia, MD, 1997.

[26] Crocco, L., and Cheng, S. I., "Theory of Combustion Instability in Liquid-Propellant Rocket Motors," AGARDograph No. 8, AGARD, Rhode-Saint-Genèse, Belgium, 1956.

[27] Lubarsky, E., and Zinn, B. T., "Heat Release Distribution in the LRE Combustor Simulator Operating in Stable and Unstable Modes," AIAA Paper 2008-1007, 2008.

E. Kim
Associate Editor